photonics

IMPACT FACTOR 2.536

CITESCORE 2.3

Article

Phase-Controlled Entanglement in a Four-Mode Optomechanical System

Cheng Jiang, Hongxia Lu, Zhangyin Zhai and Guibin Chen

Special Issue

Nonlinear and Quantum Optics in Coupled Structures: Fundamentals and Applications

Edited by

Dr. Bing He and Dr. Jianming Wen

MDPI

https://doi.org/10.3390/photonics9110818

photonics

MDPI

Article

Phase-Controlled Entanglement in a Four-Mode Optomechanical System

Cheng Jiang *, Hongxia Lu, Zhangyin Zhai and Guibin Chen

School of Physics and Electronic Electrical Engineering, Huaiyin Normal University, Huai'an 223300, China
* Correspondence: chengjiang@hytc.edu.cn

Abstract: We present a scheme for realizing phase-controlled entanglement in a microwave optomechanical system comprising two microwave cavities and two mechanical oscillators. Under specific driving conditions, we show that this optomechanical interface can be exploited to generate simultaneously the stationary cavity–cavity entanglement, mechanical–mechanical entanglement, and cavity–mechanical entanglement. Due to the closed loop interaction, we find that the entanglement can be controlled flexibly by tuning the phase difference between the optomechanical coupling strengths. The dependence of the entanglement on the amplitudes of the optomechanical coupling strengths is also explored in detail. Moreover, the bipartite entanglements are robust against temperature, and it is shown that the mechanical oscillators are cooled to the ground state in the parameter regimes for observing entanglement.

Keywords: bipartite entanglement; optomechanical system; phase difference; ground state

Citation: Jiang, C.; Lu, H.; Zhai, Z.; Chen, G. Phase-Controlled Entanglement in a Four-Mode Optomechanical System. *Photonics* **2022**, *9*, 818. https://doi.org/10.3390/photonics9110818

Received: 10 October 2022
Accepted: 26 October 2022
Published: 29 October 2022

1. Introduction

Entanglement, one essential feature of quantum mechanics, is an indispensable resource for quantum information processing. This phenomenon has been demonstrated in various systems, such as superconducting qubits [1], atomic ensembles [2,3], individual atoms [4] and ions [5], and electron spins [6]. In the past few decades, mechanical oscillators with high resonance frequencies and quality factors have been extensively explored. They can be coupled to a variety of quantum systems, including superconducting qubits [7], quantum dots [8], a single-spin qubit [9], Bose–Einstein condensate [10], and to photons at nearly arbitrary wavelength. Recently, entanglement between mechanical oscillator and atomic spin ensemble [11] as well as the phonon-mediated entanglement between two superconducting qubits [12] have been demonstrated. Therefore, hybrid mechanical systems provide a promising platform for building quantum networks [13].

Cavity optomechanical systems, where the mechanical oscillator interacts with the electromagnetic cavity via radiation pressure, can also serve as an excellent candidate for the interface that connects different components in quantum networks [14–22]. Recent milestones in this field include cooling of the mechanical oscillator to the quantum ground state [23–25] and observation of quantum effects such as optomechanical squeezing of light and mechanical motion [26–29]. Moreover, a myriad of schemes have been proposed to generate the entanglement based on optomechanical systems [30–48]. Recent optomechanical experiments have successfully demonstrated the entanglement between photons and a mechanical oscillator [49], between two mechanical oscillators [50–53], and between photons at both optical [54] and microwave [55] frequencies. Very recently, significant attention has been paid to the nonreciprocal transmission in multimode optomechanical systems with closed loop interaction [56–70], where the phase difference between the optomechanical coupling strengths can be exploited to control the direction of light propagation. In addition, it has been shown that the light-vibration entanglement can be controlled by the phase difference in three-mode optomechanical systems [71,72].

Here, we study the phase-controlled entanglement in a four-mode optomechanical system, which consists of two cavity modes coupled via two mechanical oscillators [64–68]. To generate the entanglement quantified by logarithmic negativity, the cavities are driven by four tones, including two blue tones and two red tones. By tuning the phase difference and the optomechanical coupling strengths, we show that this hybrid system provides a platform to generate simultaneously the cavity–cavity entanglement, mechanical–mechanical entanglement, and cavity–mechanical entanglement. Furthermore, we find that the stationary entanglement is robust against the environmental temperature and both the mechanical oscillators can be cooled to the ground state. Our scheme could be realized based on the current experiments [64–67].

2. Model and Theory

We consider the optomechanical system schematically shown in Figure 1a, where two cavity modes are, respectively, coupled to two mechanical oscillators via radiation pressure. The Hamiltonian of the system is given by

$$\begin{aligned} H/\hbar = & \sum_{i=1}^{2} \omega_i a_i^\dagger a_i + \sum_{i=1}^{2} \Omega_i b_i^\dagger b_i + \sum_{i=1}^{2}\sum_{j=1}^{2} g_{0,ij} a_i^\dagger a_i (b_j^\dagger + b_j) \\ & + \sum_{i=1}^{2}\sum_{j=1}^{2} \varepsilon_{ij}[a_i e^{i(\omega_{d,ij}t+\phi_{ij})} + a_i^\dagger e^{-i(\omega_{d,ij}t+\phi_{ij})}], \end{aligned} \tag{1}$$

where the first term describes the energy of the cavity modes with creation (annihilation) operators a ($a^\dagger$) and resonance frequency ω_i; the second term represents the mechanical modes with creation (annihilation) operators b ($b^\dagger$) and resonance frequency Ω_i; the third term denotes the optomechanical coupling between the cavity modes a_i and the mechanical modes b_j with $g_{0,ij}$ being the vacuum optomechanical coupling strength; and the last term corresponds to the interaction between the cavity modes and the driving fields with amplitude ε_{ij}, frequency $\omega_{d,ij}$, and phase ϕ_{ij}. We linearize the Hamiltonian by expanding cavity modes as the sum of their steady-state field amplitudes and the small fluctuations, i.e., $a_i \to a_i + \sum_{j=1}^{2} \alpha_{ij} e^{-i\omega_{d,ij}t}$, where α_{ij} is the coherent state amplitude produced in cavity i due to the drive with detuning $\Delta_{ij} = \omega_i - \omega_{d,ij}$. Here, we choose $\Delta_{11} = \Omega_1 + \delta_1$, $\Delta_{12} = -(\Omega_2 + \delta_2)$, $\Delta_{21} = -(\Omega_1 + \delta_1)$, and $\Delta_{22} = \Omega_2 + \delta_2$ with δ_i being the extra detuning from the exact red (blue) sidebands to study the entanglement in this system, as shown in Figure 1b. Moving into the rotating frame with respect to $H_0/\hbar = \sum_{i=1}^{2} \omega_i a_i^\dagger a_i + (\Omega_i + \delta_i) b_i^\dagger b_i$ and neglecting the counter-rotating and off-resonant terms under the condition of $\Omega_i, |\Omega_1 - \Omega_2| > \{\kappa_i, G_{11}, G_{22}, J_{12}, J_{21}\}$, the linearized Hamiltonian can be derived as (see details in Appendix A)

$$H/\hbar = -\sum_{i=1}^{2} \delta_i b_i^\dagger b_i + (G_{11} e^{i\phi_{11}} a_1^\dagger b_1 + J_{12} e^{i\phi_{12}} a_1^\dagger b_2^\dagger + J_{21} e^{i\phi_{21}} a_2^\dagger b_1^\dagger + G_{22} e^{i\phi_{22}} a_2^\dagger b_2 + \text{H.c}), \tag{2}$$

where $G_{11} = g_{0,11}|\alpha_{11}|$, $G_{22} = g_{0,22}|\alpha_{22}|$, $J_{12} = g_{0,12}|\alpha_{12}|$, and $J_{21} = g_{0,21}|\alpha_{21}|$ are the field-enhanced optomechanical coupling strengths. Here, we denote $G_{ij}(J_{ij})$ as the red (blue) sidebands of cavity a_i on the mechanical mode b_j. Due to the loop interaction in this optomechanical system, only the phase difference between the optomechanical coupling strengths has physical effects. By redefining the operators $a_1 \to a_1 e^{i\phi_{11}}, b_2 \to b_2 e^{i(\phi_{12}-\phi_{11})}, a_2 \to a_2 e^{i\phi_{21}}$, the Hamiltonian Equation (2) becomes

$$\begin{aligned} H/\hbar = & -\delta_1 b_1^\dagger b_1 - \delta_2 b_2^\dagger b_2 + G_{11}(a_1^\dagger b_1 + a_1 b_1^\dagger) + J_{12}(a_1^\dagger b_2^\dagger + a_1 b_2) + J_{21}(a_2^\dagger b_1^\dagger + a_2 b_1) \\ & + G_{22}(a_2^\dagger b_2 e^{-i\phi} + a_2 b_2^\dagger e^{i\phi}), \end{aligned} \tag{3}$$

with $\phi = \phi_{11} + \phi_{21} - \phi_{12} - \phi_{22}$ being the phase difference.

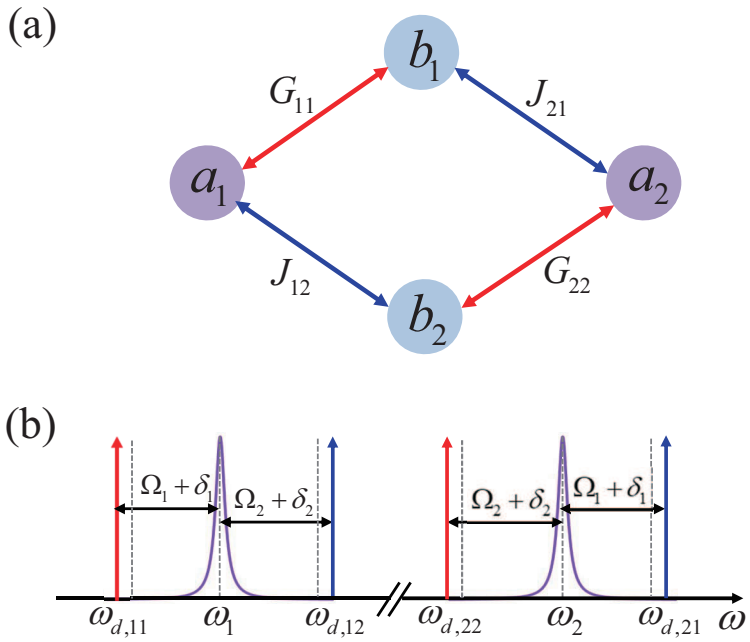

Figure 1. (**a**) Schematic of the optomechanical system. Two cavity modes a_1 and a_2 are, respectively, coupled to two mechanical modes b_1 and b_2 with the effective optomechanical coupling strengths G_{11}, J_{12}, J_{21}, and G_{22}. (**b**) Frequency domain schematic of the four-tone driving scheme. Cavity mode a_1 with resonance frequency ω_1 is driven by two tones at frequencies $\omega_{d,11} = \omega_1 - (\Omega_1 + \delta_1)$ and $\omega_{d,12} = \omega_1 + (\Omega_2 + \delta_2)$. Cavity mode a_2 with resonance frequency ω_2 is driven by two tones at frequencies $\omega_{d,21} = \omega_2 + (\Omega_1 + \delta_1)$ and $\omega_{d,22} = \omega_2 - (\Omega_2 + \delta_2)$.

According to the linearized Hamiltonian (3) and Heisenberg equation of motion, the quantum Langevin equations (QLEs) can be derived by adding the damping and input noise terms phenomenologically [64,65,67,68], which yields

$$\begin{aligned}
\dot{a_1} &= -\frac{\kappa_1}{2}a_1 - iG_{11}b_1 - iJ_{12}b_2^\dagger + \sqrt{\kappa_1}a_{1,\mathrm{in}},\\
\dot{a_2} &= -\frac{\kappa_2}{2}a_2 - iJ_{21}b_1^\dagger - iG_{22}b_2e^{-i\phi} + \sqrt{\kappa_2}a_{2,\mathrm{in}},\\
\dot{b_1} &= -\left(\frac{\gamma_1}{2} - i\delta_1\right)b_1 - iG_{11}a_1 - iJ_{21}a_2^\dagger + \sqrt{\gamma_1}b_{1,\mathrm{in}},\\
\dot{b_2} &= -\left(\frac{\gamma_2}{2} - i\delta_2\right)b_2 - iJ_{12}a_1^\dagger - iG_{22}a_2e^{i\phi} + \sqrt{\gamma_2}b_{2,\mathrm{in}},
\end{aligned} \tag{4}$$

where κ_i $(i = 1, 2)$ is the decay rate of cavity mode a_i with zero-mean noise operator $a_{i,\mathrm{in}}$, and γ_i is the damping rate of mechanical mode b_i with zero-mean operator $b_{i,\mathrm{in}}$. Defining the quadratures $U_i = (a_i + a_i^\dagger)/\sqrt{2}$, $V_i = (a_i - a_i^\dagger)/i\sqrt{2}$, $X_i = (b_i + b_i^\dagger)/\sqrt{2}$, $P_i = (b_i - b_i^\dagger)/i\sqrt{2}$, and the corresponding input noise operators $U_{i,\mathrm{in}} = (a_{i,\mathrm{in}} + a_{i,\mathrm{in}}^\dagger)/\sqrt{2}$, $V_{i,\mathrm{in}} = (a_{i,\mathrm{in}} - a_{i,\mathrm{in}}^\dagger)/i\sqrt{2}$, $X_{i,\mathrm{in}} = (b_{i,\mathrm{in}} + b_{i,\mathrm{in}}^\dagger)/\sqrt{2}$, $P_{i,\mathrm{in}} = (b_{i,\mathrm{in}} - b_{i,\mathrm{in}}^\dagger)/i\sqrt{2}$, the linearized QLEs can be written in the following compact matrix form:

$$\dot{\mu}(t) = A\mu(t) + n(t), \tag{5}$$

where $\mu(t) = (U_1(t), V_1(t), U_2(t), V_2(t), X_1(t), P_1(t), X_2(t), P_2(t))^T$ is the vector of the fluctuation operators, $n(t) = (\sqrt{\kappa_1}U_{1,\mathrm{in}}(t), \sqrt{\kappa_1}V_{1,\mathrm{in}}(t), \sqrt{\kappa_2}U_{2,\mathrm{in}}(t), \sqrt{\kappa_2}V_{2,\mathrm{in}}(t), \sqrt{\gamma_1}X_{1,\mathrm{in}}(t), \sqrt{\gamma_1}P_{1,\mathrm{in}}(t), \sqrt{\gamma_2}X_{2,\mathrm{in}}(t), \sqrt{\gamma_2}P_{2,\mathrm{in}}(t))^T$ is the vector of the corresponding noises, and the coefficient matrix

$$A = \begin{pmatrix} -\kappa_1/2 & 0 & 0 & 0 & 0 & G_{11} & 0 & -J_{12} \\ 0 & -\kappa_1/2 & 0 & 0 & -G_{11} & 0 & -J_{12} & 0 \\ 0 & 0 & -\kappa_2/2 & 0 & 0 & -J_{21} & -G_{22}\sin\phi & G_{22}\cos\phi \\ 0 & 0 & 0 & -\kappa_2/2 & -J_{21} & 0 & -G_{22}\cos\phi & -G_{22}\sin\phi \\ 0 & G_{11} & 0 & -J_{21} & -\gamma_1/2 & -\delta_1 & 0 & 0 \\ -G_{11} & 0 & -J_{21} & 0 & \delta_1 & -\gamma_1/2 & 0 & 0 \\ 0 & -J_{12} & G_{22}\sin\phi & G_{22}\cos\phi & 0 & 0 & -\gamma_2/2 & -\delta_2 \\ -J_{12} & 0 & -G_{22}\cos\phi & G_{22}\sin\phi & 0 & 0 & \delta_2 & -\gamma_2/2 \end{pmatrix}. \quad (6)$$

The formal solution of Equation (5) is

$$\mu(t) = M(t)\mu(0) + \int_0^t dsM(s)n(t-s), \quad (7)$$

where

$$M(t) = \exp\{At\}. \quad (8)$$

The system is stable when all of the eigenvalues of A have negative real parts, which can be derived from the Routh–Hurwitz criterion [73]. When the stability conditions are fulfilled, one can obtain $M(\infty) = 0$ in the steady state.

The steady state of the system is a zero-mean Gaussian state due to the linearized dynamics and the Gaussian nature of the input quantum noises, which is fully characterized by an 8×8 correlation matrix (CM) V, with its components

$$V_{ij} = [\langle \mu_i(\infty)\mu_j(\infty) + \mu_j(\infty)\mu_i(\infty)\rangle]/2. \quad (9)$$

When the system is stable, by substituting Equation (7) into Equation (9), we can obtain

$$V_{ij} = \sum_{k,l}\int_0^\infty ds \int_0^\infty ds' M_{ik}(s)M_{jl}(s')\Phi_{kl}(s-s'), \quad (10)$$

where $\Phi_{kl}(s-s') = (\langle n_k(s)n_k(s') + n_l(s')n_k(s)\rangle)/2 = D_{kl}\delta(s-s')$. According to the correlation functions that the noise operators satisfy,

$$\begin{aligned} &\langle a_{i,\mathrm{in}}(s)a^\dagger_{i,\mathrm{in}}(s')\rangle = \delta(s-s'), \langle a^\dagger_{i,\mathrm{in}}(s')a_{i,\mathrm{in}}(s)\rangle = 0, \\ &\langle b_{i,\mathrm{in}}(s)b^\dagger_{i,\mathrm{in}}(s')\rangle = (n_{m,i}+1)\delta(s-s'), \langle b^\dagger_{i,\mathrm{in}}(s')b_{i,\mathrm{in}}(s)\rangle = n_{m,i}\delta(s-s'), \end{aligned} \quad (11)$$

where $n_{m,i} = \{\exp[\hbar\Omega_i/(k_\mathrm{B}T)] - 1\}^{-1}$ denotes the thermal phonon number of the mechanical mode b_i with k_B being the Boltzmann constant and T being the environment temperature, we can obtain $D = \mathrm{Diag}[\kappa_1/2, \kappa_1/2, \kappa_2/2, \kappa_2/2, (2n_{m,1}+1)\gamma_1/2, (2n_{m,1}+1)\gamma_1/2, (2n_{m,2}+1)\gamma_2/2, (2n_{m,2}+1)\gamma_2/2]$, and Equation (10) becomes $V = \int_0^\infty dsM(s)DM(s)^T$. The time evolution of the correlation matrix V satisfies $\dot{V}(t) = AV(t) + V(t)A^T + D$ [36]. In the steady state, the correlation matrix V fulfills the Lyapunov equation [30]:

$$AV + VA^T = -D, \quad (12)$$

which is a linear equation for V and can be straightforwardly solved for given parameters in matrix A and matrix D; but the general analytical expression is too cumbersome to be reported here. The bipartite entanglement between different modes can be quantified by the logarithmic negativity [30,31,74]

$$E_N = \max[0, -\ln 2\eta^-], \quad (13)$$

where $\eta^- \equiv 2^{-1/2}\{\Sigma(V_\mathrm{bp}) - [\Sigma(V_\mathrm{bp})^2 - 4\det V_\mathrm{bp}]^{1/2}\}^{1/2}$, with $\Sigma(V_\mathrm{bp}) \equiv \det B + \det B' - 2\det C$. The reduced CM V_bp contains the entries of V, and it can be obtained by selecting

the rows and columns of the interesting mode in V. By writing the reduced CM $V_{\rm bp}$ in a 2×2 block form, we have

$$V_{\rm bp} \equiv \begin{pmatrix} B & C \\ C^T & B' \end{pmatrix}. \tag{14}$$

Note that matrix A in Equation (6) contains the phase difference ϕ; hence, the correlation matrix V and the logarithmic negativity E_N depend on ϕ. We will study how to control the entanglement quantified by Equation (13) in this optomechanical system by tuning the phase difference ϕ.

Furthermore, based on the correlation matrix V, the final average phonon numbers in the mechanical modes b_1 and b_2 can be calculated by

$$\begin{aligned} \langle b_1^\dagger b_1 \rangle &= n_1^f = \frac{V_{5,5} + V_{6,6} - 1}{2}, \\ \langle b_2^\dagger b_2 \rangle &= n_2^f = \frac{V_{7,7} + V_{8,8} - 1}{2}, \end{aligned} \tag{15}$$

which affect the quantum entanglement in the hybrid system.

3. Results and Discussion

In this section, we choose the parameters from a recent experiment to demonstrate the numerical results about the phase-controlled entanglement in this system. The parameters are [65] $\Omega_1/2\pi = 4.34$ MHz, $\Omega_2/2\pi = 5.64$ MHz, $\kappa_1/2\pi = 2.42$ MHz, $\kappa_2/2\pi = 1.98$ MHz, $\gamma_1/2\pi = 40$ Hz, $\gamma_2/2\pi = 80$ Hz, and $T = 20$ mK. The system works in the resolved sideband regime and the rotating-wave approximation is valid.

In Figure 2, we plot the logarithmic negativity E_N between (a) the two cavity modes as well as (b) the two mechanical modes versus the optomechanical coupling strength $G_{22}/2\pi$ and the phase difference ϕ/π. At $G_{22} = 0$, the optomechanical interactions cannot form a closed loop and the phase-dependent effect is absent. With the increase in the coupling strength G_{22}, it is evident that the quantum entanglement depends on the phase difference ϕ. Note that cavity mode a_1 is driven on the blue (red) sideband of the mechanical mode b_2 (b_1), while cavity mode a_2 is driven on the blue (red) sideband of the mechanical mode b_1 (b_2). Therefore, the parametric-amplifier interaction $J_{12}(a_1^\dagger b_2^\dagger + a_1 b_2)$ entangles a_1 and b_2, and the interaction $J_{21}(a_2^\dagger b_1^\dagger + a_2 b_1)$ entangles a_2 and b_1. Moreover, the beam-splitter interaction $G_{11}(a_1^\dagger b_1 + a_1 b_1^\dagger)$ swaps a_1 and b_1, and the interaction $G_{22}(a_2^\dagger b_2 e^{-i\phi} + a_2 b_2^\dagger e^{i\phi})$ swaps a_2 and b_2. Consequently, the two cavity modes can be entangled via the routes $a_1 \leftrightarrow b_1 \leftrightarrow a_2$ and $a_1 \leftrightarrow b_2 \leftrightarrow a_2$, and the two mechanical modes can also be entangled via the routes $b_1 \leftrightarrow a_1 \leftrightarrow b_2$ and $b_1 \leftrightarrow a_2 \leftrightarrow b_2$, where the phase difference ϕ plays a vital role. At $\phi = \pi$, we can see that both the cavity–cavity and mechanical–mechanical entanglement firstly decrease from an initial value to zero when G_{22} increases. With further increasing G_{22} above a critical value, it is shown that the quantum entanglement starts to increase again. This phenomenon is closely related to the quantum interference between the eigenmodes of the system [34].

We proceed to study the effect of the entangling-interaction strength J_{12} on the entanglement in Figure 3, assuming $J_{21} = J_{12}$ for simplicity. Figure 3a and Figure 3c plot, respectively, the dynamics of the cavity–cavity entanglement and mechanical–mechanical entanglement for $\phi = 0, \pi/2$, and π. It is shown that stationary entanglement can be achieved after $t \approx 2$ μs, which depends on the phase difference ϕ. Moreover, Figure 3b and Figure 3d plot the stationary cavity–cavity entanglement and mechanical–mechanical entanglement as functions of the entangling-interaction strength $J_{12}/2\pi$ for different values of phase difference ϕ. At $\phi = 0$, both the cavity–cavity entanglement and the mechanical–mechanical entanglement are enhanced monotonically with the increase in the coupling strength J_{12} in the parameter regimes. When the phase difference ϕ is tuned to be $\pi/2$ or π, the stationary logarithmic negativity E_N becomes larger and reaches the maximum with the increase of J_{12}. With further increasing J_{12}, the entanglement will decrease and be zero above a critical value of J_{12}. On one hand, it is straightforward that the entanglement

can be enhanced by increasing the coupling strengths J_{12} (J_{21}), which are strengthened by the blue-detuned driving fields. On the other hand, increasing J_{12} (J_{21}) can suppress the cavity-cooling effect for given G_{12} (G_{21}) and increase the effective temperature of the cavity and mechanical modes, which will reduce the entanglement. In addition, when the coupling strengths J_{12} and J_{21} are too strong, the system will become unstable. Therefore, the maximum entanglement is achieved by balancing these two competing effects [35]. Throughout this work, we have checked numerically that the chosen parameters satisfy the stability condition.

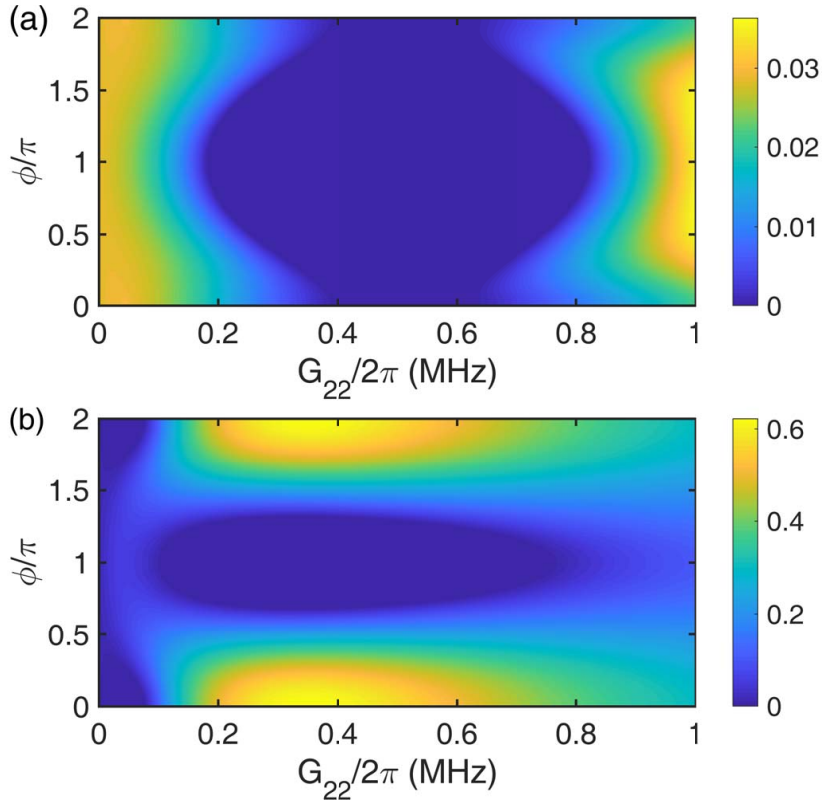

Figure 2. Contour plots of the logarithmic negativity E_N between (**a**) the two cavity modes and (**b**) the two mechanical modes as functions of the coupling strength $G_{22}/2\pi$ and the phase difference ϕ/π. Parameters are $\Omega_1/2\pi = 4.34$ MHz, $\Omega_2/2\pi = 5.64$ MHz, $\kappa_1/2\pi = 2.42$ MHz, $\kappa_2/2\pi = 1.98$ MHz, $\gamma_1/2\pi = 40$ Hz, $\gamma_2/2\pi = 80$ Hz, $\delta_1 = \delta_2 = 0$, $G_{11}/2\pi = 0.5$ MHz, $J_{21} = J_{12} = 2\pi \times 0.15$ MHz, and $T = 20$ mK.

Furthermore, we study the phase dependence of the optomechanical entanglement in Figure 4. The logarithmic negativity E_N between the two cavity modes is plotted as a function of the phase difference ϕ for different values of J_{12} in Figure 4a. At $J_{12}/(2\pi) = 0.1$ MHz, the maximum cavity–cavity entanglement is achieved around $\phi = \pi$ and the minimum value locates at $\phi = 0$ (2π). However, when the value of J_{12} is increased to be 0.2 MHz and 0.25 MHz, the peak around $\phi = \pi$ turns into a dip. Especially, the cavity–cavity entanglement in the vicinity of $\phi = \pi$ is absent for $J_{12} = 0.25$ MHz. Therefore, the phase difference ϕ can be exploited as a switch of the cavity–cavity entanglement between zero and nonzero value. Similarly, Figure 4b plots the logarithmic negativity E_N between the two mechanical modes versus the phase difference ϕ. It is shown that the mechanical–mechanical entanglement reaches the minimum at $\phi = \pi$ and the maximum at $\phi = 0$ (2π) for $J_{12}/2\pi = 0.1$, 0.2, and 0.25 MHz. Moreover, the entanglement can be strengthened monotonically by increasing the coupling strength J_{12} at $\phi = 0$ (2π). Consequently, the quantum entanglement can be controlled by the phase difference in this optomechanical system.

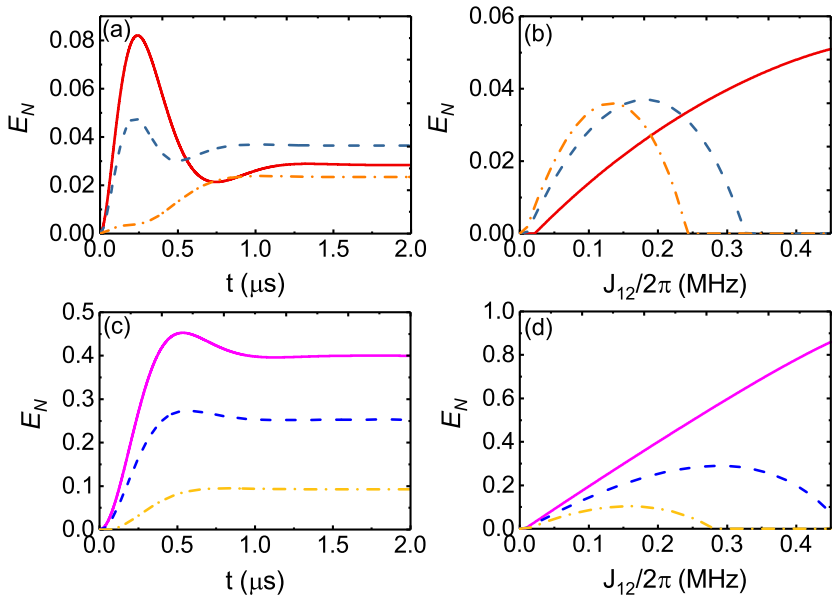

Figure 3. Logarithmic negativity E_N affected by the phase difference ϕ. (**a**) Time evolution of the logarithmic negativity E_N between the cavity modes a_1 and a_2 with $J_{12}/2\pi = 0.2$ MHz for $\phi = 0, \pi/2$, and π. (**b**) Stationary logarithmic negativity E_N between the cavity modes a_1 and a_2 as a function of $J_{12}/2\pi$ for $\phi = 0, \pi/2$, and π. (**c**) Time evolution of the logarithmic negativity E_N between the mechanical modes b_1 and b_2 with $J_{12}/2\pi = 0.2$ MHz for $\phi = 0, \phi = \pi/2$, and $\phi = \pi$. (**d**) Stationary logarithmic negativity E_N between the mechanical modes b_1 and b_2 as a function of $J_{12}/2\pi$ for $\phi = 0$, $\pi/2$, and π. Here, $\phi = 0, \pi/2, \pi$ correspond to the solid line, dashed line, and dash-dotted line, respectively. Other parameters are the same as Figure 2, except $G_{22}/2\pi = 1$ MHz. Here, we keep $J_{21} = J_{12}$.

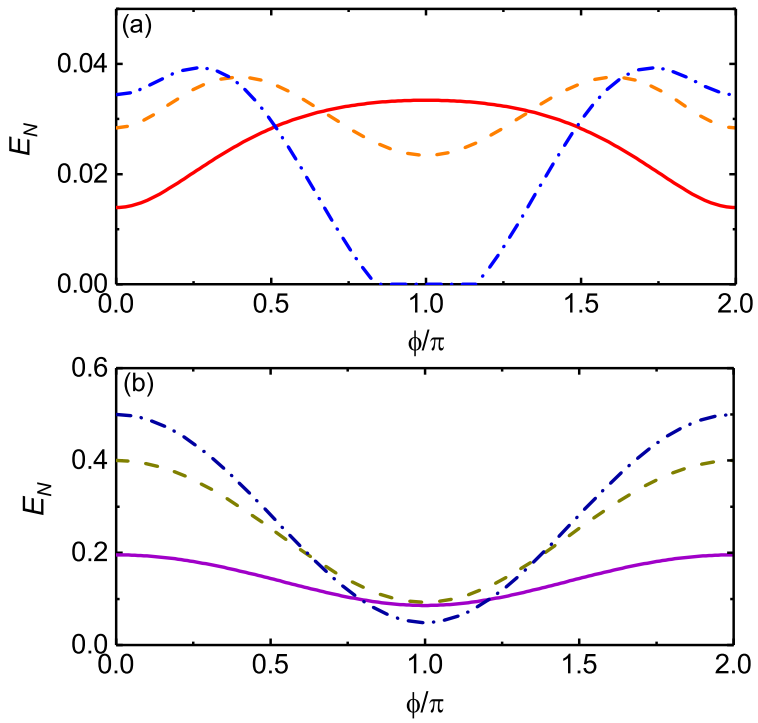

Figure 4. Plots of the logarithmic negativity E_N between (**a**) the two cavity modes and (**b**) the two mechanical modes versus the phase difference ϕ/π for $J_{12}/2\pi = 0.1$ MHz (solid lines), 0.2 MHz (dashed lines), and 0.25 MHz (dash-dotted lines). The other parameters are the same as those in Figure 3.

As mentioned above, the entanglement between the two cavity (mechanical) modes is realized via the entanglement transfer between the cavity and mechanical modes. In Figure 5, we study the optomechanical entanglement between the cavity mode a_1 (a_2) and mechanical mode b_2 (b_1). Figure 5a plots the time evolution of the logarithmic negativity E_N between the cavity mode a_1 and mechanical mode b_2 with $J_{12}/2\pi = 0.15$ MHz for different values of phase difference ϕ. It is shown that stationary entanglement can be achieved after $t \approx 2$ μs and it is strengthened when the the phase difference ϕ is increased from 0 to π. The logarithmic negativity E_N between a_1 and b_2 versus the entangling-interaction strength J_{12} is plotted in Figure 5b, which shows that stationary entanglement can be enhanced by increasing the strength J_{12} and reaches the maximum at some critical value for $\phi = 0$ and $\pi/2$. In the chosen parameter regime, the stationary entanglement increases monotonically with the increase in J_{12} for $\phi = \pi$. In addition, Figure 5c plots the time evolution of the logarithmic negativity E_N between a_2 and b_1 for $\phi = 0, \pi/2$, and π, where stationary entanglement can also be obtained. The stationary entanglement between a_2 and b_1 versus J_{12} is plotted in Figure 5d, where the maximum entanglement is achieved around $J_{12}/2\pi = 0.15$ MHz for various phase differences. Figure 5 also shows that the stationary entanglement between a_2 and b_1 is weaker than the entanglement between a_1 and b_2, which is mainly due to $G_{22} > G_{11}$ under consideration.

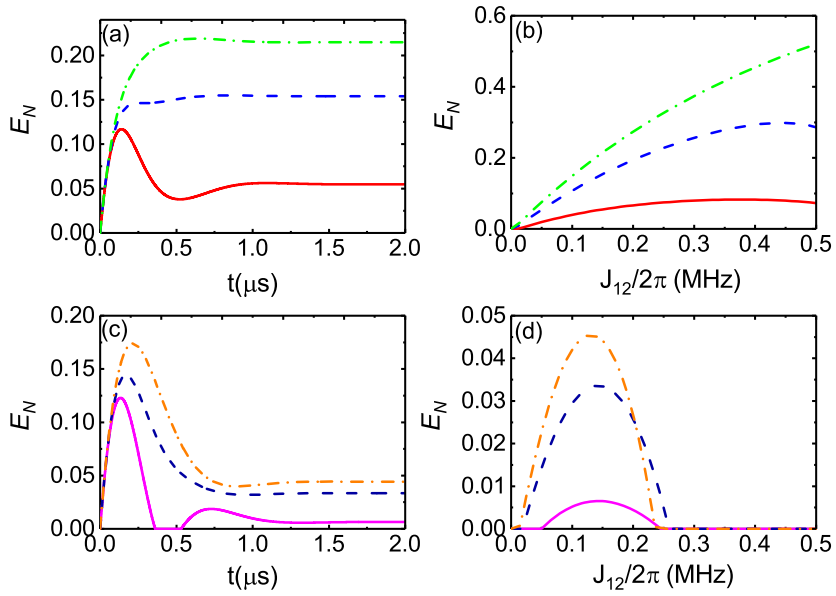

Figure 5. Logarithmic negativity E_N between the cavity and mechanical modes affected by the phase difference ϕ. (**a**) Time evolution of the logarithmic negativity E_N between the cavity mode a_1 and mechanical mode b_2 with $J_{12}/2\pi = 0.15$ MHz for $\phi = 0$, $\pi/2$, and π. (**b**) Stationary logarithmic negativity E_N between the cavity mode a_1 and mechanical mode b_2 as a function of $J_{12}/2\pi$ for various phase differences. (**c**) Time evolution of the logarithmic negativity E_N between the cavity mode a_2 and mechanical mode b_1 with $J_{12}/2\pi = 0.15$ MHz for $\phi = 0$, $\pi/2$, and π. (**d**) Stationary logarithmic negativity E_N between the cavity mode a_2 and mechanical mode b_1 versus the $J_{12}/2\pi$ for various phase differences. Here, the solid line, dashed line, and dash-dotted line represent $\phi = 0$, $\pi/2$, and π, respectively. The other parameters are the same as those in Figure 3.

The robustness of the quantum entanglement with respect to the environmental temperature is shown in Figure 6. The value of E_N decreases with the increasing temperature for various phase differences. Figure 6a plots the logarithmic negativity E_N between the cavity modes a_1 and a_2 versus the temperature T. At $\phi = 0$, the cavity–cavity entanglement persists up to 150 mK. The entanglement vanishes at higher temperature for $\phi = \pi/2$ and $\phi = \pi$. The entanglement between the two mechanical modes shown in Figure 6b is stronger than the cavity–cavity entanglement and survives at higher temperature. In addition, the entanglement between the cavity mode a_1 and mechanical mode b_2 versus the

temperature is plotted in Figure 6c, where $E_N \approx 0.11$ can be obtained for $T = 400$ mK and $\phi = \pi$. The logarithmic negativity E_N between the cavity mode a_2 and mechanical mode b_1 is much smaller than the value in Figure 6c and survives at much lower temperature, which results from $G_{22} > G_{11}$. The value of E_N between a_2 and b_1 can be increased by reducing G_{22}, but the entanglement between the two cavity (mechanical) modes will be absent in some parameter regimes shown in Figure 2.

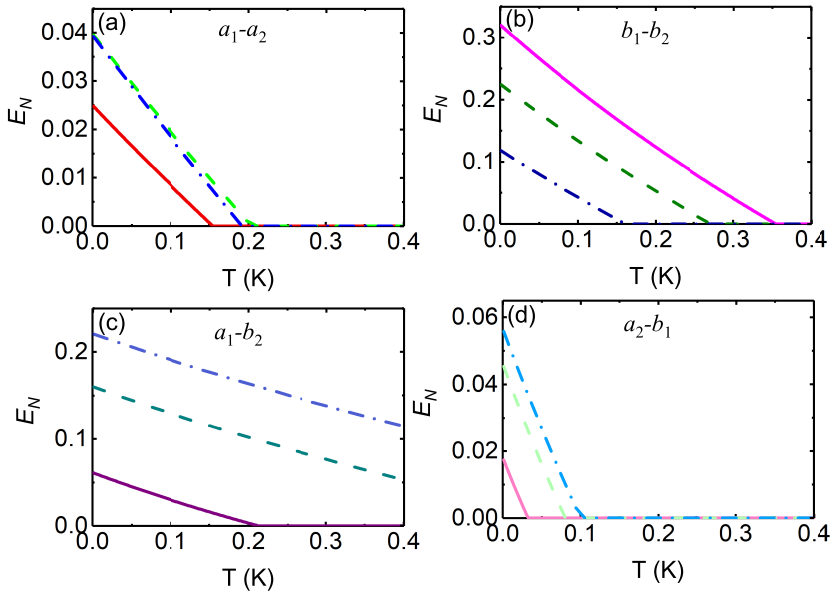

Figure 6. Plots of logarithmic negativity E_N as functions of the environment temperature T for $\phi = 0$ (solid lines), $\pi/2$ (dashed lines), and π (dash-dotted lines). Panel (**a**) represents the entanglement between the two cavity modes, panel (**b**) represents the entanglement between the two mechanical modes, panel (**c**) corresponds to the entanglement between the cavity mode a_1 and mechanical mode b_2, and panel (**d**) corresponds to the entanglement between the cavity mode a_2 and mechanical mode b_1. The other parameters are the same as those in Figure 3, except $J_{12}/2\pi = J_{21}/2\pi = 0.15$ MHz.

Finally, the entanglement usually survives at low final phonon numbers. The beam-splitter interaction such as $G_{11}(a_1^\dagger b_1 + a_1 b_1^\dagger)$ can not only result in state transfer between a_1 and b_1 but also cool the mechanical mode b_1. In Figure 7, we numerically study the final average phonon numbers n_1^f and n_2^f by choosing the parameters for observing the entanglement mentioned above. Figure 7a plots the phonon numbers n_1^f and n_2^f as a function of the optomechanical coupling strength $J_{12}/2\pi$ with $\phi = 0$, which shows that both n_1^f and n_2^f increase monotonically with the enhancement of J_{12}. The parametric-amplifier interaction $J_{12}(a_1^\dagger b_2^\dagger + a_1 b_2)$ is caused by driving the cavity mode a_1 on the blue sideband of mechanical mode b_2, where a drive photon is scattered into a photon at frequency ω_1 and a phonon at frequency Ω_2, resulting in the monotonic increase in phonon number at larger J_{12}. It is noted that quantum phase transition in the two-mode Rabi model has been recently investigated by analyzing the eigenenergy of the system [75], but quantum phase transition of the phonon number of the mechanical mode in optomechanical systems has seldom been reported. In addition, here, we show that both n_1^f and n_2^f are smaller than 1 in the chosen parameter regime. Therefore, simultaneous cooling of the mechanical modes and quantum entanglement can be realized in this optomechanical system. In addition, the phase dependence of phonon numbers is plotted in Figure 7b. The final average phonon numbers of the two mechanical modes reach the maximum at $\phi = \pi$ and the minimum at $\phi = 0$ (2π), which is contrary to the entanglement between the two mechanical modes shown in Figure 4b.

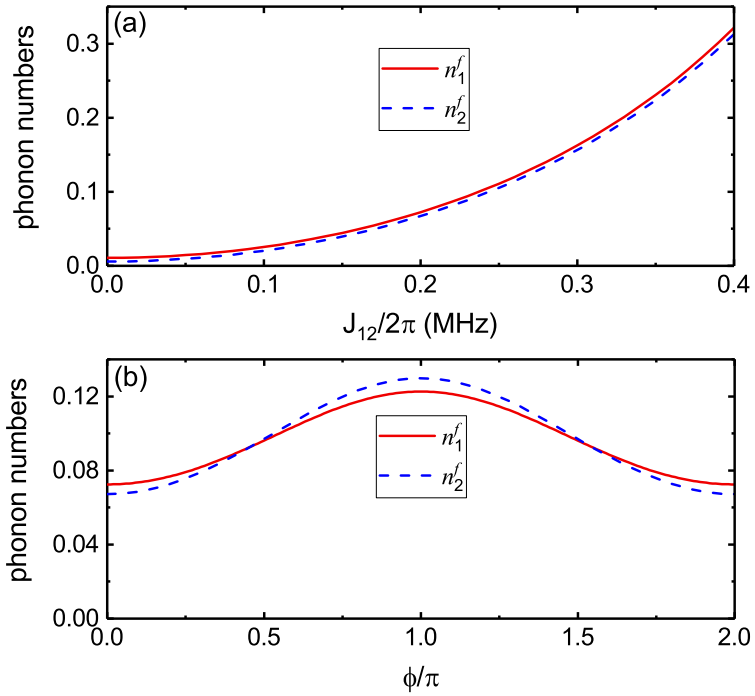

Figure 7. The final average phonon numbers n_1^f (solid line) and n_2^f (dashed line) versus (**a**) the optomechanical coupling strength $J_{12}/2\pi$ with $\phi = 0$ and (**b**) the phase difference ϕ/π with $J_{12}/2\pi = J_{21}/2\pi = 0.2$ MHz. The other parameters are the same as those in Figure 3.

4. Conclusions

In conclusion, we have explored the phase-controlled entanglement in a multimode optomechanical system, where two cavity modes are, respectively, coupled to two mechanical modes via radiation pressure. Four tones are applied to the cavity modes to generate the entanglement, where each cavity is driven on the red sideband and blue sideband of the two mechanical modes, respectively. The dynamics of the bipartite entanglement is studied, which shows that the stationary entanglement can be generated. We have shown that the entanglement can be effectively modulated by the phase difference between the optomechanical coupling strengths that form a loop interaction. By tuning the optomechanical coupling strengths and phase difference in some parameter regimes, we can realize simultaneously the entanglement between the two cavity mode, between the two mechanical modes, and between the cavity and mechanical modes. We also find that the entanglement is robust against temperature and the mechanical resonators can be cooled to the ground state when the entanglement is generated.

Author Contributions: Conceptualization and model, C.J.; numerical simulation, H.L. and Z.Z.; writing—original draft preparation, C.J.; writing—review and editing, G.C. and C.J. All authors have read and agreed to the published version of the manuscript.

Funding: This research was supported by National Natural Science Foundation of China (No: 11874170), Qinglan Project of Jiangsu Province of China, and Natural Science Research of Jiangsu Higher Education Institutions of China (19KJA150011).

Institutional Review Board Statement: Not applicable.

Informed Consent Statement: Not applicable.

Data Availability Statement: Not applicable.

Conflicts of Interest: The authors declare no conflict of interest.

Appendix A. Derivation of the Linearized Hamiltonian

We can linearize the Hamiltonian Equation (1) by the following two steps:

(1) Expanding the cavity modes as the sum of their steady-state field amplitudes and the small fluctuations [64,65,67,68], i.e., $a_i \to a_i + \sum_{j=1}^{2} \alpha_{ij} e^{-i\omega_{d,ij}t}$, where α_{ij} is the coherent state amplitude produced in cavity i due to the drive. Then, we can obtain the following approximation:

$$a_i^\dagger a_i \approx a_i^\dagger \sum_{j=1}^{2} \alpha_{ij} e^{-i\omega_{d,ij}t} + a_i \sum_{j=1}^{2} \alpha_{ij}^* e^{i\omega_{d,ij}t}. \tag{A1}$$

(2) Moving into the interaction picture with respect to [64,65,67,68],

$$H_0/\hbar = \sum_{i=1}^{2} \omega_i a_i^\dagger a_i + (\Omega_i + \delta_i) b_i^\dagger b_i, \tag{A2}$$

the linearized Hamiltonian becomes

$$\begin{aligned} H/\hbar &= -\sum_{i=1}^{2} \delta_i b_i^\dagger b_i + \sum_{i=1}^{2}\sum_{j=1}^{2} g_{0,ij} \left(a_i^\dagger \sum_{j=1}^{2} \alpha_{ij} e^{-i\omega_{d,ij}} e^{i\omega_i t} + a_i \sum_{j=1}^{2} \alpha_{ij}^* e^{i\omega_{d,ij}t} e^{-i\omega_i t} \right) \left[b_j^\dagger e^{i(\Omega_j+\delta_j)t} + b_j e^{-i(\Omega_j+\delta_j)t} \right] \\ &= -\sum_{i=1}^{2} \delta_i b_i^\dagger b_i + \sum_{i=1}^{2}\sum_{j=1}^{2} g_{0,ij} \left[a_i^\dagger (\alpha_{i1} e^{i\Delta_{i1}t} + \alpha_{i2} e^{i\Delta_{i2}}) + a_i (\alpha_{i1}^* e^{-i\Delta_{i1}t} + \alpha_{i2}^* e^{-i\Delta_{i2}t}) \right] \left[b_j^\dagger e^{i(\Omega_j+\delta_j)t} + b_j e^{-i(\Omega_j+\delta_j)t} \right] \\ &= -\sum_{i=1}^{2} \delta_i b_i^\dagger b_i + g_{0,11}\alpha_{11} a_1^\dagger b_1 + g_{0,11}\alpha_{11}^* a_1 b_1^\dagger + g_{0,12}\alpha_{12} a_1^\dagger b_2^\dagger + g_{0,12}\alpha_{12}^* a_1 b_2 + g_{0,21}\alpha_{21} a_2^\dagger b_1^\dagger + g_{0,21}\alpha_{21}^* a_2 b_1 \\ &\quad + g_{0,22}\alpha_{22} a_2^\dagger b_2 + g_{0,22}\alpha_{22}^* a_2 b_2^\dagger + H_{\mathrm{RWA}} + H_{\mathrm{off}}, \end{aligned} \tag{A3}$$

where H_{RWA} describes the rapidly oscillating terms at frequencies $\pm 2[\Omega_{1(2)} + \delta_{1(2)}]$ and $\pm(\Omega_1 + \delta_1 + \Omega_2 + \delta_2)$, and H_{off} denotes the off-resonant terms oscillating at $\pm(\Omega_1 + \delta_1 - \Omega_2 - \delta_2)$. Here, $\Delta_{ij} = \omega_i - \omega_{d,ij}$ is the detuning of the drive tone with respect to cavity a_i, and we consider the situation where

$$\Delta_{11} = \Omega_1 + \delta_1, \Delta_{12} = -(\Omega_2 + \delta_2), \Delta_{21} = -(\Omega_1 + \delta_1), \Delta_{22} = \Omega_2 + \delta_2. \tag{A4}$$

Under the condition $\Omega_i, |\Omega_1 - \Omega_2| > \{\kappa_i, G_{11}, G_{22}, J_{12}, J_{21}\}$, the rotation wave approximation (RWA) can be applied and the off-resonant terms can be ignored. Defining $g_{0,11}\alpha_{11} = G_{11}e^{i\phi_{11}}$, $g_{0,22}\alpha_{22} = G_{22}e^{i\phi_{22}}$, $g_{0,12}\alpha_{12} = J_{12}e^{i\phi_{12}}$, and $g_{0,21}\alpha_{21} = J_{21}e^{i\phi_{21}}$ as the field-enhanced optomechanical coupling strengths, the linearized Hamiltonian can be written as

$$H/\hbar = -\sum_{i=1}^{2} \delta_i b_i^\dagger b_i + (G_{11}e^{i\phi_{11}} a_1^\dagger b_1 + J_{12}e^{i\phi_{12}} a_1^\dagger b_2^\dagger + J_{21}e^{i\phi_{21}} a_2^\dagger b_1^\dagger + G_{22}e^{i\phi_{22}} a_2^\dagger b_2 + \mathrm{H.c}), \tag{A5}$$

which is Equation (2) in the main text.

References

1. Berkley, A.J.; Xu, H.; Ramos, R.C.; Gubrud, M.A.; Strauch, F.W.; Johnson, P.R.; Anderson, J.R.; Dragt, A.J.; Lobb, C.J.; Wellstood, F.C. Entangled macroscopic quantum states in two superconducting qubits. *Science* **2003**, *300*, 1548–1550. [CrossRef] [PubMed]
2. Julsgaard, B.; Kozhekin, A.; Polzik, E.S. Experimental long-lived entanglement of two macroscopic objects. *Nature* **2001**, *413*, 400–403. [CrossRef] [PubMed]
3. Chou, C.W.; Riedmatten, H.; Felinto, D.; Polyakov, S.V.; van Enk, S.J.; Kimble, H.J. Measurement-induced entanglement for excitation stored in remote atomic ensembles. *Nature* **2005**, *438*, 828–832. [CrossRef]
4. Ritter, S.; Nölleke, C.; Hahn, C.; Reiserer, A.; Neuzner, A.; Uphoff, M.; Mücke, M.; Figueroa, E.; Bochmann, J.; Rempe, G. An elementary quantum network of single atoms in optical cavities. *Nature* **2012**, *484*, 195–200. [CrossRef]
5. Moehring, D.L.; Maunz, P.; Olmschenk, S.; Younge, K.C.; Matsukevich, D.N.; Duan, L.-M.; Monroe, C. Entanglement of single-atom quantum bits at a distance. *Nature* **2007**, *449*, 68–71. [CrossRef]

6. Hensen, B.; Bernien, H.; Dréau, A.E.; Reiserer, A.; Kalb, N.; Blok, M.S.; Ruitenberg, J.; Vermeulen, R.F.L.; Schouten, R.N.; Abellán, C.; et al. Loophole-free Bell inequality violation using electron spins separated by 1.3 kilometres. *Nature* **2015**, *526*, 682–686. [CrossRef]
7. O'Connell, A.D.; Hofheinz, M.; Ansmann, M.; Bialczak, R.C.; Lenander, M.; Lucero, E.; Neeley, M.; Sank, D.; Wang, H.; Weides, M.; et al. Quantum ground state and single-phonon control of a mechanical resonator. *Nature* **2010**, *464*, 697–703. [CrossRef]
8. Yeo, I.; Assis, P.L.; Gloppe, A.; Dupont-Ferrier, E.; Verlot, P.; Malik, N.S.; Dupuy, E.; Claudon, J.; Gérard, J.-M.; Auffèves, A.; et al. Strain-mediated coupling in a quantum dot-mechanical oscillator system. *Nat. Nanotechnol.* **2014**, *9*, 106–110. [CrossRef]
9. Kolkowitz, S.; Jayich, A.C.B.; Unterreithmeier, Q.P.; Bennett, S.D.; Rabl, P.; Harris, J.G.E.; Lukin, M.D. Coherent sensing of a mechanical resonator with a single-spin qubit. *Science* **2012**, *335*, 1603–1606. [CrossRef]
10. Hunger, D.; Camerer, S.; Hänsch, T.W.; König, D.; Kotthaus, J.P.; Reichel, J.; Treutlein, P. Resonant coupling of a Bose-Einstein Condensate to a micromechanical oscillator. *Phys. Rev. Lett.* **2010**, *104*, 143002. [CrossRef]
11. Thomas, R.A.; Parniak, M.; Østfeldt, C.; Møller, C.B.; Bærentsen, C.; Tsaturyan, Y.; Schliesser, A.; Appel, J.; Zeuthen, E.; Polzik, E.S. Entanglement between distant macroscopic mechanical and spin systems. *Nat. Phys.* **2021**, *17*, 228–233. [CrossRef]
12. Bienfait, A.; Satzinger, K.J.; Zhong, Y.P.; Chang, H.S.; Chou, M.H.; Conner, C.R.; Dumur, E.; Grebel, J.; Peairs, G.A.; Povey, R.G.; et al. Phonon-mediated quantum state transfer and remote qubit entanglement. *Science* **2019**, *364*, 368–371. [CrossRef] [PubMed]
13. Kimble, H.J. The quantum internet. *Nature* **2008**, *453*, 1023–1030. [CrossRef] [PubMed]
14. Aspelmeyer, M.; Kippenberg, T.J.; Marquardt, F. Cavity optomechanics. *Rev. Mod. Phys.* **2014**, *86*, 1391–1452. [CrossRef]
15. Stannigel, K.; Rabl, P.; Sørensen, A.S.; Zoller, P.; Lukin, M.D. Optomechanical transducers for long-distance quantum communication. *Phys. Rev. Lett.* **2010**, *105*, 220501. [CrossRef]
16. Wang, Y.D.; Clerk, A.A. Using interference for high fidelity quantum state transfer in optomechanics. *Phys. Rev. Lett.* **2012**, *108*, 153603. [CrossRef]
17. Tian, L. Adiabatic state conversion and pulse transmission in optomechanical systems. *Phys. Rev. Lett.* **2012**, *108*, 153604. [CrossRef]
18. Barzanjeh, S.; Abdi, M.; Milburn, G.J.; Tombesi, P.; Vitali, D. Reversible optical-to-microwave quantum interface. *Phys. Rev. Lett.* **2012**, *109*, 130503. [CrossRef]
19. Andrews, R.W.; Peterson, R.W.; Purdy, T.P.; Cicak, K.; Simmonds, R.W.; Regal, C.A.; Lehnert, K.W. Bidirectional and efficient conversion between microwave and optical light. *Nat. Phys.* **2014**, *10*, 321–326. [CrossRef]
20. Dong, C.H.; Wang, Y.D.; Wang, H.L. Optomechanical interfaces for hybrid quantum networks. *Natl. Sci. Rev.* **2015**, *2*, 510–519. [CrossRef]
21. Forsch, M.; Stockill, R.; Wallucks, A.; Marinković, I.; Gärtner, C.; Norte, R.A.; van Otten, F.; Fiore, A.; Srinivasan, K.; Gröblacher, S. Microwave-to-optics conversion using a mechanical oscillator in its quantum ground state. *Nat. Phys.* **2020**, *16*, 69–74. [CrossRef] [PubMed]
22. Jiang, W.T.; Sarabalis, C.J.; Dahmani, Y.D.; Patel, R.N.; Mayor, F.M.; McKenna, T.P.; Laer, R.V.; Safavi-Naeini, A.H. Efficient bidirectional piezo-optomechanical transduction between microwave and optical frequency. *Nat. Commun.* **2020**, *11*, 1166. [CrossRef] [PubMed]
23. Teufel, J.D.; Donner, T.; Li, D.; Harlow, J.W.; Allman, M.S.; Cicak, K.; Sirois, A.J.; Whittaker, J.D.; Lehnert, K.W.; Simmonds, R.W. Sideband cooling of micromechanical motion to the quantum ground state. *Nature* **2011**, *475*, 359–363. [CrossRef] [PubMed]
24. Chan, J.; Alegre, T.P.M.; Safavi-Naeini, A.H.; Hill, J.T.; Krause, A.; Gröblacher, S.; Aspelmeyer, M.; Painter, O. Laser cooling of a nanomechanical oscillator into its quantum ground state. *Nature* **2011**, *478*, 89–92. [CrossRef] [PubMed]
25. Delić, U.; Reisenbauer, M.; Dare, K.; Grass, D.; Vuletic, V.; Kiesel, N.; Aspelmeyer, M. Cooling of a levitated nanoparticle to the motional quantum ground state. *Science* **2020**, *367*, 892–895. [CrossRef]
26. Safavi-Naeini, A.H.; Gröblacher, S.; Hill, J.T.; Chan, J.; Aspelmeyer, M.; Painter, O. Squeezed light from a silicon micromechanical resonator. *Nature* **2013**, *500*, 185–189. [CrossRef]
27. Purdy, T.P.; Yu, P.L.; Peterson, R.W.; Kampel, N.S.; Regal, C.A. Strong optomechanical squeezing of light. *Phys. Rev. X* **2013**, *3*, 031012. [CrossRef]
28. Wollman, E.E.; Lei, C.U.; Weinstein, A.J.; Suh, J.; Kronwald, A.; Marquardt, F.; Clerk, A.A.; Schwab, K.C. Quantum squeezing of motion in a mechanical resonator. *Science* **2015**, *349*, 952–955. [CrossRef]
29. Pirkkalainen, J.M.; Damskägg, E.; Brandt, M.; Massel, F.; Sillanpää, M.A. Squeezing of quantum noise of motion in a micromechanical resonator. *Phys. Rev. Lett.* **2015**, *115*, 243601. [CrossRef]
30. Vitali, D.; Gigan, S.; Ferreira, A.; Böhm, H.R.; Tombesi, P.; Guerreiro, A.; Vedral, V.; Zeilinger, A.; Aspelmeyer, M. Optomechanical entanglement between a movable mirror and a cavity field. *Phys. Rev. Lett.* **2007**, *98*, 030405. [CrossRef]
31. Genes, C.; Mari, A.; Tombesi, P.; Vitali, D. Robust entanglement of a micromechanical resonator with output optical fields. *Phys. Rev. A* **2008**, *78*, 032316. [CrossRef]
32. Barzanjeh, S.; Vitali, D.; Tombesi, P.; Milburn, G.J. Entangling optical and microwave cavity modes by means of a nanomechanical resonator. *Phys. Rev. A* **2011**, *84*, 042342. [CrossRef]
33. Kuzyk, M.C.; Enk, S.J.; Wang, H.L. Generating robust optical entanglement in weak-coupling optomechanical systems. *Phys. Rev. A* **2013**, *88*, 062341. [CrossRef]

34. Tian, L. Robust photon entanglement via quantum interference in optomechanical interfaces. *Phys. Rev. Lett.* **2013**, *110*, 233602. [CrossRef]
35. Wang, Y.D.; Clerk, A.A. Reservoir-engineered entanglement in optomechanical systems. *Phys. Rev. Lett.* **2013**, *110*, 253601. [CrossRef] [PubMed]
36. Wang, G.L.; Huang, L.; Lai, Y.C.; Grebogi, C. Nonlinear dynamics and quantum entanglement in optomechanical systems. *Phys. Rev. Lett.* **2014**, *112*, 110406. [CrossRef]
37. Liao, J.Q.; Wu, Q.Q.; Nori, F. Entangling two macroscopic mechanical mirrors in a two-cavity optomechanical system. *Phys. Rev. A* **2014**, *89*, 014302. [CrossRef]
38. Wang, M.; Lu, X.Y.; Wang, Y.D.; You, J.Q.; Wu, Y. Macroscopic quantum entanglement in modulated optomechanics. *Phys. Rev. A* **2016**, *94*, 053807. [CrossRef]
39. Sun, F.X.; Mao, D.; Dai, Y.T.; Ficek, Z.; He, Q.Y.; Gong, Q.H. Phase control of entanglement and quantum steering in a three-mode optomechanical system. *New J. Phys.* **2017**, *19*, 123039. [CrossRef]
40. Li, J.; Li, G.; Zippilli, S.; Vitali, D.; Zhang, T. Enhanced entanglement of two different mechanical resonators via coherent feedback. *Phys. Rev. A* **2017**, *95*, 043819. [CrossRef]
41. Qin, L.G.; Wang, Z.Y.; Ma, H.Y.; Zhang, C.M.; Ren, L.; Wang, L.L.; Gong, S.Q. Optomechanical entanglement switch in the hybrid opto-electromechanical device. *JOSA B* **2019**, *36*, 1544–1550. [CrossRef]
42. Hu, C.S.; Liu, Z.Q.; Liu, Y.; Shen, L.T.; Wu, H.; Zheng, S.B. Entanglement beating in a cavity optomechanical system under two-field driving. *Phys. Rev. A* **2020**, *101*, 033810. [CrossRef]
43. Zhang, Y.L.; Yang, C.S.; Shen, Z.; Dong, C.H.; Guo, G.C.; Zou, C.L.; Zou, X.B. Enhanced optomechanical entanglement and cooling via dissipation engineering. *Phys. Rev. A* **2020**, *101*, 063836. [CrossRef]
44. Zhong, C.C.; Han, X.; Tang, H.X.; Jiang L.; Entanglement of microwave-optical modes in a strongly coupled electro-optomechanical system. *Phys. Rev. A* **2020**, *101*, 032345. [CrossRef]
45. Li, G.Y.; Nie, W.J.; Wu, Y.; Liao, Q.; Chen, A.; Lan, Y. Manipulating the steady-state entanglement via three-level atoms in a hybrid levitated optomechanical system. *Phys. Rev. A* **2020**, *102*, 063501. [CrossRef]
46. Jiao, Y.F.; Zhang, S.D.; Zhang, Y.L.; Miranowicz, A.; Kuang, L.M.; Jing, H. Nonreciprocal optomechanical entanglement against backscattering losses. *Phys. Rev. Lett.* **2020**, *125*, 143605. [CrossRef]
47. Lin, Q.; He, B.; Xiao, M. Entangling two macroscopic mechanical resonators at high temperature. *Phys. Rev. Appl.* **2020**, *13*, 034030. [CrossRef]
48. Jiang, C.; Tserkis, S.; Collins, K.; Onoe, S.; Li, Y.; Tian, L. Switchable bipartite and genuine tripartite entanglement via an optoelectromechanical interface. *Phys. Rev. A* **2020**, *101*, 042320. [CrossRef]
49. Palomaki, T.A.; Teufel, J.D.; Simmonds, R.W.; Lehnert, K.W. Entangling mechanical motion with microwave fields. *Science* **2013**, *342*, 710–713. [CrossRef]
50. Ockeloen-Korppi, C.F.; Damskägg, E.; Pirkkalainen, J.M.; Asjad, M.; Clerk, A.A.; Massel, F.; Woolley, M.J.; Sillanpää, M.A. Stabilized entanglement of massive mechanical oscillators. *Nature* **2018**, *556*, 478–482. [CrossRef]
51. Riedinger, R.; Wallucks, A.; Marinković, I.; Löschnauzer, C.; Aspelmeyer, M.; Hong, S.; Gröblacher, S. Remote quantum entanglement between two micromechanical oscillators. *Nature* **2018**, *556*, 473–477. [CrossRef]
52. de Lépinay, L.M.; Ockeloen-Korppi, C.F.; Woolley, M.J.; Sillanpää, M.A. Quantum mechanics–free subsystem with mechanical oscillators. *Science* **2021**, *372*, 625. [CrossRef] [PubMed]
53. Kotler, S.; Peterson, G.A.; Shojaee, E.; Lecocq, F.; Cicak, K.; Kwiatkowski, A.; Geller, S.; Glancy, S.; Knill, E.; Simmonds, R.W.; et al. Direct observation of deterministic macroscopic entanglement. *Science* **2021**, *372*, 622. [CrossRef] [PubMed]
54. Chen, J.X.; Rossi, M.; Mason, D.; Schliesser, A. Entanglement of propagating optical modes via a mechanical interface. *Nat. Commun.* **2020**, *11*, 943. [CrossRef]
55. Barzanjeh, S.; Redchenko, E.S.; Peruzzo, M.; Wulf, M.; Lewis, D.P.; Arnold, G.; Fink, J.M. Stationary entangled radiation from micromechanical motion. *Nature* **2019**, *570*, 480–483. [CrossRef] [PubMed]
56. Xu, X.W.; Li, Y.; Chen, A.X.; Liu Y. Nonreciprocal conversion between microwave and optical photons in electro-optomechanical systems. *Phys. Rev. A* **2016**, *93*, 023827. [CrossRef]
57. Li, Y.; Huang, Y.Y.; Zhang, X.Z.; Tian, L. Optical directional amplification in a three-mode optomechanical system. *Opt. Express* **2017**, *25*, 18907. [CrossRef]
58. Zhang, X.Z.; Tian, L.; Li, Y. Optomechanical transistor with mechanical gain. *Phys. Rev. A* **2018**, *97*, 043818. [CrossRef]
59. Tian, L.; Li, Z. Nonreciprocal quantum-state conversion between microwave and optical photons. *Phys. Rev. A* **2017**, *96*, 013808. [CrossRef]
60. Jiang, C.; Song, L.N.; Li, Y. Directional amplifier in an optomechanical system with optical gain. *Phys. Rev. A* **2018**, *97*, 053812. [CrossRef]
61. Ruesink, F.; Miri, M.A.; Alù, A.; Verhagen, E. Nonreciprocity and magnetic-free isolation based on optomechanical interactions. *Nat. Commun.* **2016**, *7*, 13662. [CrossRef]
62. Miri, M.A.; Ruesink, F.; Verhagen, E.; Alù, A. Optical nonreciprocity based on optomechanical coupling. *Phys. Rev. Appl.* **2017**, *7*, 064014. [CrossRef] [PubMed]
63. Fang, K.J.; Luo, J.; Metelmann, A.; Matheny, M.H.; Marquardt, F.; Clerk, A.A.; Painter, O. Generalized non-reciprocity in an optomechanical circuit via synthetic magnetism and reservoir engineering. *Nat. Phys.* **2017**, *13*, 465. [CrossRef]

64. Bernier, N.R.; Tóth, L.D.; Koottavida, A.; Ioannou, M.A.; Malz, D.; Nunnenkamp, A.; Feofanov, A.K.; Kippenberg, T.J. Nonreciprocal reconfigurable microwave optomechanical circuit. *Nat. Commun.* **2017**, *8*, 604. [CrossRef]
65. Barzanjeh, S.; Wulf, M.; Peruzzo, M.; Kalaee, M.; Dieterle, P.B.; Painter, O.; Fink, J.M. Mechanical on-chip microwave circulator. *Nat. Commun.* **2017**, *8*, 953. [CrossRef] [PubMed]
66. Peterson, G.A.; Lecocq, F.; Cicak, K.; Simmonds, R.W.; Aumentado, J.; Teufel, J.D. Demonstration of efficient nonreciprocity in a microwave optomechanical circuit. *Phys. Rev. X* **2017**, *7*, 031001. [CrossRef]
67. de Lépinay, L.M.; Damskägg, E.; Ockeloen-Korppi, C.F.; Sillanpää, M.A. Realization of directional amplification in a microwave optomechanical device. *Phys. Rev. Appl.* **2019**, *11*, 034027. [CrossRef]
68. Malz, D.; Tóth, L.D.; Bernier, N.R.; Feofanov, A.K.; Kippenberg, T.J.; Nunnenkamp, A. Quantum-limited directional amplifiers with optomechanics. *Phys. Rev. Lett.* **2018**, *120*, 023601. [CrossRef]
69. Shen, Z.; Zhang, Y.L.; Chen, Y.; Sun, F.W.; Zou, X.B.; Guo, G.C.; Zou, C.L.; Dong, C.H. Reconfigurable optomechanical circulator and directional amplifier. *Nat. Commun.* **2018**, *9*, 1797. [CrossRef]
70. Ruesink, F.; Mathew, J.P.; Miri, M.A.; Alù, A.; Verhagen, E. Optical circulation in a multimode optomechanical resonator. *Nat. Commun.* **2018**, *9*, 1798. [CrossRef]
71. Lai, D.G.; Liao, J.Q.; Miranowicz, A.; Nori, F. Noise-tolerant optomechanical entanglement via synthetic magnetism. *Phys. Rev. Lett.* **2022**, *129*, 063602. [CrossRef]
72. Liu, J.X.; Jiao, Y.F.; Li, Y.; Xu, X.W.; He, Q.Y., Jing, H. Phase-controlled asymmetric optomechanical entanglement against defect losses. *arXiv* **2022**, arXiv:2209.12508. [CrossRef] [PubMed]
73. DeJesus, E.X.; Kaufman, C. Routh-Hurwitz criterion in the examination of eigenvalues of a system of nonlinear ordinary differential equations. *Phys. Rev. A* **1987**, *35*, 5288. [CrossRef] [PubMed]
74. Adesso, G.; Serafini, A. Illuminati, F. Extremal entanglement and mixedness in continuous variable systems. *Phys. Rev. A* **2004**, *70*, 022318.
75. Shen, L.T.; Yang, J.W.; Zhong, Z.R.; Yang, Z.B.; Zheng, S.B. Quantum phase transition and quench dynamics in the two-mode Rabi model. *Phys. Rev. A* **2021**, *104*, 063703.